*Friction* **11**(11): 2008–2020 (2023)
https://doi.org/10.1007/s40544-022-0704-8
ISSN 2223-7690
CN 10-1237/TH
RESEARCH ARTICLE

# Current-carrying friction in carbon coated ball bearing

**Peidong XUE**[1,2], **Cheng CHEN**[1], **Xue FAN**[1,*], **Dongfeng DIAO**[1,*]

[1] *Institute of Nanosurface Science and Engineering (INSE), Guangdong Provincial Key Laboratory of Micro/Nano Optomechatronics Engineering, Shenzhen University, Shenzhen 518060, China*

[2] *College of Physics and Optoelectronic Engineering, Shenzhen University, Shenzhen 518060, China*

*Received: 31 December 2021 / Revised: 02 July 2022 / Accepted: 03 October 2022*



**Abstract:** In this work, we proposed a method for coating the whole surfaces of bearing balls uniformly by carbon film with a rotatable ball clamp. We studied the carbon/carbon friction with a self-designed current-carrying ball bearing friction test system. A notable and instant friction force drop of 28% and significant carbon film wear alleviation were found when currents were applied. By using TEM-, SEM-, and EDS-analysis, special carbon stacks with a mixture of large wear particles and oxide were found in the wear areas under current applied condition. We elucidated the current-carrying friction mechanisms as follows: (1) wear particles formation; (2) wear particles charged by tribomicroplasma; (3) formation of surface passivated carbon stacks under electric force; (4) sliding between passivated carbon surfaces. This work may facilitate the development of novel solid-lubricated ball bearings and lay some foundations for current-carrying rolling friction.

**Keywords:** current-carrying friction; carbon film; ball bearing; carbon stack

## 1 Introduction

With the fast development of electric vehicles [1] and high-speed railways [2], the friction performances under external electric field or with current passing states have become an important issue that draws a lot of attentions. Under complicated electric environments, failure can occur on all contact/sliding surfaces of components. Clarifying the current-carrying induced physical or chemical reactions at the friction interface is important for improving the reliability and lifetime of the related devices [3–5]. Besides sliding conditions, ball bearings in electric vehicles may also work under current-carrying conditions [6]. It is reported that the electrostatic charges accumulation at the ball bearings can lead to degradation of lubricant and the current induced by breakdown would induce morphology damage [7, 8]. Enhancing the conductivity of the lubricated interface is a solution to alleviate charge accumulation, which asks for new conductive lubricating materials in bearings [9].

Using conductive solid lubrication is a possible solution to eliminate charge accumulation. The tribological properties of many solid lubrication materials, including AgI, Ag/C, Cu/C, graphite, and carbon nanotube films under electrical contact situations have been extensively studied [10–12]. Among these materials, carbon materials could have good tribological properties and high electric conductivity simultaneously owing to their tunable $sp^2/sp^3$ structures [13, 14]. It was found that current could reduce the friction coefficient but increase the wear rate when metals slided against diamond like carbon (DLC) or transition metal dichalcogenides [15, 16]. As reasons for friction reduction of carbon materials under current-carrying condition, two major mechanisms are proposed. It was found that in the current-carrying friction between graphite/graphite, the friction force would drop in reactive atmosphere but increase in inert atmosphere [17, 18]. Thus, the dangling bonds passivation of carbon atoms with gas adsorption was considered as the reason for the friction force reduction [19]. Recently,

* Corresponding authors: Xue FAN, E-mail: fanx@szu.edu.cn; Dongfeng DIAO, E-mail: dfdiao@szu.edu.cn

our group found that in the steel/amorphous carbon film (a-C film) current-carrying friction condition, the current would facilitate the formation of transfer film and induce the transformation of amorphous carbon into graphene nanocrystallites in the transfer film, which could also reduce the friction force [20, 21]. As for rolling friction condition, the fast change of the contact points makes the physical or chemical reactions at friction interface to be very transient. Clarifying the current-carrying rolling friction would be helpful to prompt the development of solid-lubricated ball bearings.

In this work, we investigated the current-carrying friction in carbon coated ball bearings. Bearing balls, as well as inner races and outer rings of the ball bearings were all coated with a-C film, which were achieved by special designed coating clamps. The effects of currents on the friction force and wear were studied. TEM-, SEM-, and EDS-analysis were conducted on the bearing ball surface to reveal the effects of current. The mechanisms of the current-induced friction reduction and wear alleviation were discussed and elucidated.

## 2 Experiments

An electron cyclotron resonance (ECR) plasma sputtering system was used to deposit a-C film on the bearing balls as well as the inner races and outer rings of the ball bearings. The process of depositing a-C film on the surfaces of bearing balls and the assembling-process of the carbon coated ball bearing as well as the current-carrying friction test system are shown in Fig. 1. The detailed descriptions of the sputtering system were reported in our previous works [22, 23]. In order to realize the a-C film deposition, divergent electron cyclotron resonance (DECR) plasma sputtering type was used [22]. The background pressure of the vacuum chamber was pumped down to $8\times10^{-5}$ Pa and then argon was inflated to keep the pressure at $1\times10^{-5}$ Pa during the deposition process. –500 V voltages were applied on the carbon target to attract ion bombardment for carbon atom sputtering. Ion-irradiation-assisted deposition process was achieved by applying a substrate bias voltage of –10 V.

Figure 1(a) presents the process of depositing a-C film on bearing balls. Different clamps were used during the deposition processes for different parts of ball bearings. The ball clamp includes four "P" shape tracks with slopes and edges. During the deposition process, the ball clamp was fixed on a rotatable substrate holder and the substrate holder was set to rotate with a rotation rate of 15 rpm. Each track could set 4 bearing balls for one deposition process. The bearing balls can roll in the tracks, which have slopes to provide different rolling axes for the balls and edges to prevent the balls from falling out of the tracks. During the deposition process, bearing balls will roll in the tracks with the 4 sequences as presented in the figure. NSK 7006C super precision bearings were used as the test samples in our experiment. The original bearing balls were replaced by 304 stainless balls with the same diameter of 7.144 mm, because the 304 stainless balls are non-magnetic and can be characterized by TEM. The deposition time was 2 hours to guarantee uniform carbon film on the 304 stainless balls. The deposition time for the other parts was also set as 2 hours.

Figure 1(b) shows the assembling-process of a carbon coated ball bearing. The original ball bearing was dispatched into four major parts including inner race of the bearing, outer ring, cage, and bearing balls (rollers) firstly. Then, all four parts were washed in hot water with chemical cleaner to remove the grease in the ball bearing. At the same time, original bearing balls were replaced by 304 stainless balls for satisfying the TEM characterization requirements. After grease was removed, all the parts were put into an ultrasonic cleaner with acetone bath for 20 minutes and then heated to 100 °C to remove the residual water. After that, the 304 stainless balls as well as the inner race and outer ring were coated with a-C film as mentioned before. After the deposition process, all the carbon-coated parts and cage were assembled together.

The self-designed current-carrying carbon coated ball bearing friction test system is shown in Fig. 1(c). The test system contains three major parts including a spindle, a tested carbon coated ball bearing, and a plastic shell. On one side of the shell, a short stick was fixed and a string was tied with the stick at the end. The angle between the string and the stick was set to be 90 degree. The other end of the string was

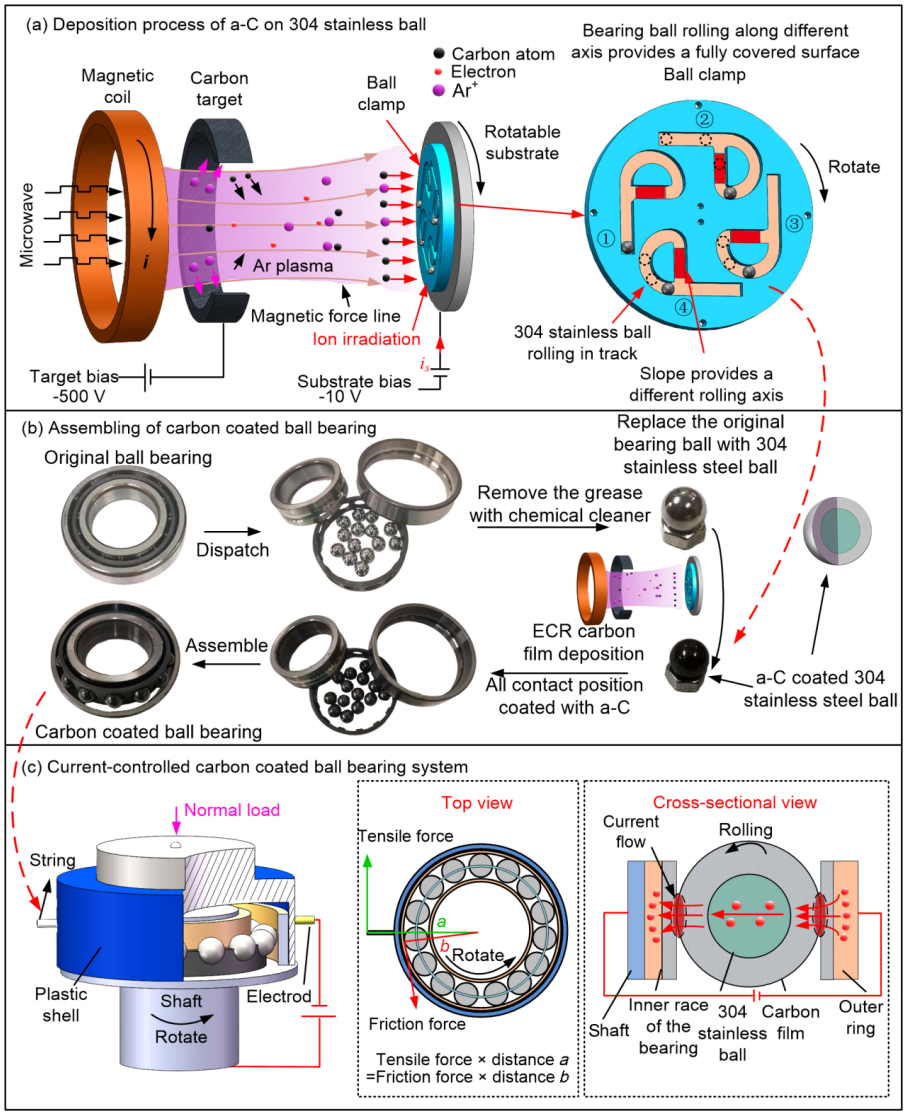


**Fig. 1** Fabrication processes of the carbon coated ball bearings and current-carry friction test system. Schematic of (a) process of depositing ECR a-C film on bearing balls as well as the ball clamp, (b) assembling-process of carbon coated ball bearing, and (c) friction test system for current-carrying carbon coated ball bearing.

tied with a strain gauge sensor (KYOWA LTS-50GA), which was used to measure the strain force generated by the friction force between the ball bearing and the shell induced torque. It is clear that the moment of the strain force equals to the moment of the friction force. Thus, the friction force can be calculated by the measured strain force, as shown in the top view in Fig. 1(c). On the other side of the shell, an electrode was installed and set to contact with the outer ring of the carbon coated ball bearing. And the shaft was designed to contact with the inner race of the carbon coated ball bearing. Thus, a circuit was built through the electrode on the shell, the outer ring, the bearing balls, the inner race, and the shaft, which can also be seen in the cross-sectional view in Fig 1(c). When voltage was applied to the test system, current would flow through the real contact positions in the ball bearing.

Frictional tests of the carbon coated ball bearing were conducted with the mentioned test system. The normal loads were set to be 3 N, 6 N, 9 N. The rotation rates of the shaft were set to be 200 rpm, 600 rpm, and 900 rpm. A constant voltage source with 12 V and a slide rheostat were used to control the current to be 0 A, 2 A, and 4 A. All the tests were conducted in a clean room with a stable temperature of 24 °C and

a relative humidity of 45%–50%. The wear stability tests were conducted with a normal load of 15 N, rotation rate of 300 rpm, and current of 4 A. The friction tests under different parameters were conducted for 5 times.

The nanostructures of the as-deposited carbon films on the ball and the worn surface of the ball were analyzed with optical microscopy, Raman spectroscopy (HORIBA, HR-Resolution, wavelength of 532 nm), scanning electron microscopy (SEM, FEI, Scios), and transmission electron microscopy (TEM, FEI, Titan3 Themis G2). Cross-sectional TEM specimens were cut from the balls and progressively thinned to about 100 nm thick by using a focused ion beam (FIB, FEI, Scios). Au and Pt protective layers were deposited on the top of the specimen subsequentially and the final polishing was done with a beam current of 27 pA to avoid possible damages or thermal recrystallization caused by ion bombardments. Energy dispersive X-ray spectroscopy (EDS) was conducted at the same time when SEM and TEM characterizations were done.

## 3 Results and discussion

### 3.1 Characterizations of carbon coated ball bearings

Figure 2 shows the characterization results of the bearing ball after coated with a-C film. As can be seen in Fig. 2(a), the a-C film coated bearing balls have a good gloss, which indicates a relative smooth surface. Figure 2(b) shows the optical photo of a bearing ball. Although the machining marks can still be observed, the whole area has been coated with carbon film. The local area was flat without any notable defect, as shown in Fig. 2(c) with the SEM characterization. Figure 2(d) shows the Raman spectrum characterized from 1,100 to 3,500 $cm^{-1}$, only a coupled band could be observed around 1,500 $cm^{-1}$, which indicates a typical structure of amorphous film [24]. The ratio of D peak to G peak intensity ($I_D/I_G$) was calculated to be 0.72. The thickness of the a-C film on the bearing ball was characterized by TEM, as shown in Fig 2(e). The carbon film thickness of the presented ball was 90 nm. Two other balls were presented in Fig. S1 in the Electronic Supplementary Material (ESM), which showed the average thickness of the film was around 91±4 nm. The high resolution TEM image presented in Fig. 2(e) confirms the amorphous structure of the film. The characterization of the bearing balls proved that the balls were coated with homogeneous a-C film. And the results also showed that the deposition method presented was an effective way for coating uniform carbon film on the whole surfaces of balls. After coated with carbon film, the resistances of the bearings between inner races and outer rings increased slightly from the original 0.4±0.2 Ω to 0.9±0.2 Ω, which was due

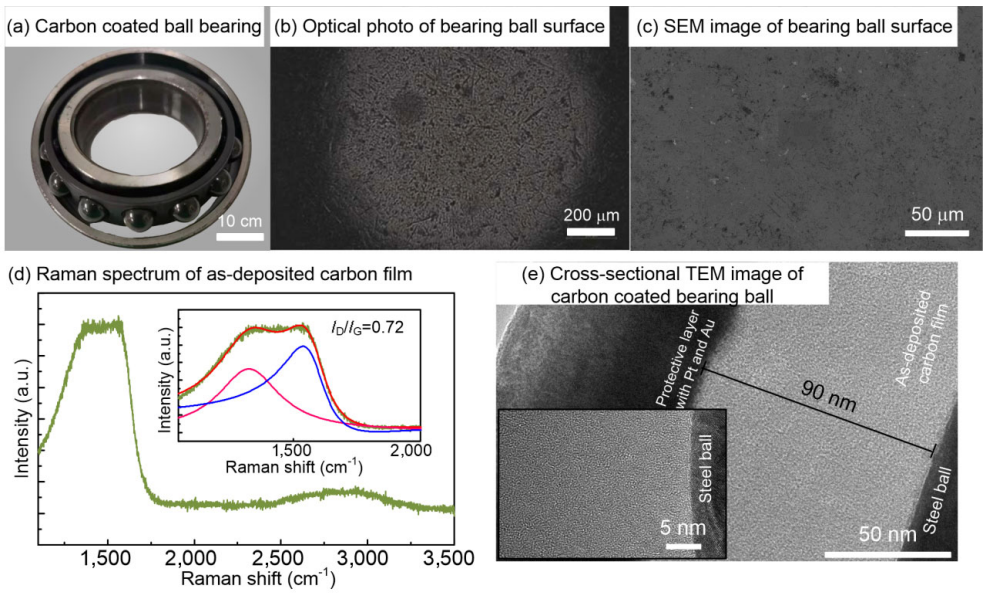


**Fig. 2** Characterization of carbon film on bearing balls. (a) Photo of the ball bearing. (b) Optical image, (c) SEM image, (d) Raman spectrum, and (e) low magnification TEM image and the inset figure is high magnification TEM image of the a-C film coated bearing ball.

to the high $sp^2$ content of the carbon film fabricated with low energy ion irradiation condition in ECR system [25]. Thus, current could flow homogeneously through the real contact areas in the ball bearings.

### 3.2 Current-carrying friction tests

#### 3.2.1 *Friction tests under different parameters*

Figure 3 presents the friction force curves under different test conditions. The grease lubricated ball bearing, which was insulated, had the highest friction force as shown in Fig. 3(a). It can be explained that under this shaft rotation rate, the ball bearing did not reach its critical lubrication condition, which made the grease an obstacle hindering the movements of the bearing balls. As for the carbon coated ball bearing, the friction force decreased notably from an average 0.27 N to an average 0.07 N with the same normal load of 6 N comparing with that of grease lubricated ball bearing, as shown in Fig. 3(b).

Figure 3(c) presents the friction force curve of the carbon coated ball bearing under the test condition of 9 N normal loads, 4 A current, and shaft rotation rate of 200 rpm. The red line in the figure was calculated by processing the original data with a low pass filter with a cut-off frequency of 0.1 Hz, which was aimed at making the influence of current to be observed clearly. It could be seen that in the first 120 s, the friction force kept in a relative stable value around 0.07 N. When 4 A current was applied, the friction force instantly dropped 28% to an average value of 0.05 N. Finally, when the current was cut off, the friction force increased immediately. Under other currents and loads, this phenomenon could also be observed, as presented in Fig. S2 in the ESM. And such current-induced instant friction drop was also found in carbon/steel sliding friction interface as our former work reported [20]. Thus, a direct relation between current and friction force in the carbon coated ball bearing system could be concluded. And it was shown that the influence of current on the friction in carbon coated ball bearing system was an instantaneous process, considering that the contact positions would change time by time in the ball bearing. The influences of different parameters on the friction force drop rates were further studied and presented in Fig. 3(d). It could be found that when the same current was applied, a higher normal load could induce a more notable friction force drop. When the normal load was kept unchanged, a higher applied current could

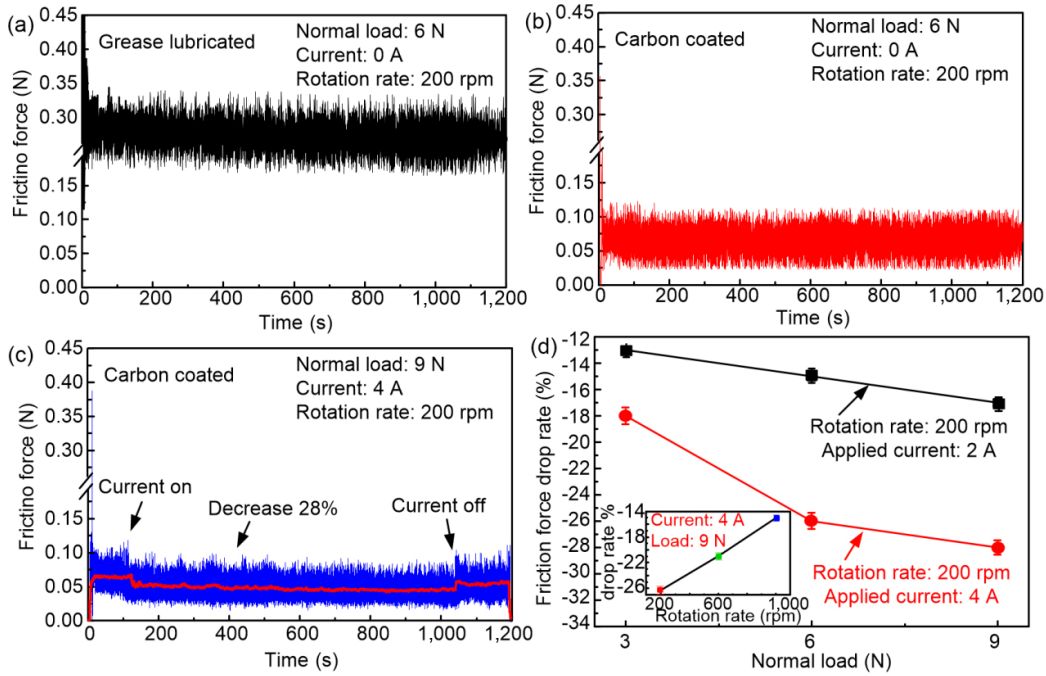


**Fig. 3** Friction force curves under different test conditions. Friction forces curves of (a) original grease lubricated bearing, (b) carbon coated bearing without current, and (c) carbon coated bearing with the friction parameters of 9 N, 4A, and 200 rpm. (d) Friction force drop rates under different normal loads, currents, and shaft rotation rates (inset figure).

lead to further decrease of the friction force. Besides, it was also found that for a constant normal load and current, an increase of the shaft rotation rate would hinder the current induced friction force decrease.

### 3.2.2 *Wear stability tests*

Figure 4 presents the friction force curves of the carbon coated ball bearing during 4 hours wear stability tests. Figure 4(a) shows the carbon coated ball bearing under the normal load of 15 N without current applied. It could be seen that with the wear stability test continuing, the friction force slightly increased and some sudden jumps of the friction force could be observed. While for the current applied situation, the friction force became more stable, as shown in Fig. 4(b). During the whole test, the friction force kept on a relative low value and no sudden jump of the friction force could be observed. Besides, the friction force curve of a pure steel ball bearing with current applied condition was also presented in Fig. 4(b). It is shown that the friction force of pure steel bearing became unstable within 20 minutes, which proves the importance of the carbon coating on the ball bearing under the current-carrying working condition. It should be mentioned that current would also induce a slight drop of friction force for pure steel ball bearings, which might be induced by the oxidation formation on the steel surface [26]. But without the protection of carbon film, the friction force of the bearing became unstable in a relative short time, which further confirms the effects of carbon film coating, as shown in Fig. S3 in the ESM.

## 3.3 Analyses for bearing balls after current-carrying frictional tests

### 3.3.1 *Optical, SEM, EDS, and Raman analyses*

Figure 5 presents the optical images, SEM images, EDS images, and Raman spectra of the a-C film coated bearing balls after wear stability tests. Figures 5(a) and 5(b) exhibit the SEM images of the bearing ball surfaces after 1 hour wear stability tests under normal load of 15 N without current applied and with 4 A current applied, respectively. The inset pictures were the optical images of the same bearing balls. For the no current condition, it could be observed that large part of the carbon film was worn and the white steel surface was exposed, as shown in Fig. 5(a). While for the current-carrying condition, as shown in Fig. 5(b), most of the surface was still covered with black carbon film and only some small white spots could be observed, which indicates the exposure of steel. Some small humps were marked with red circles in both of the SEM and optical photos in Fig. 5(b). These humps were carbon stacks formed around the local spalling area of the carbon film.

Figures 5(c) and 5(d) exhibit the SEM images of the bearing ball surfaces after 4 hour wear stability tests under normal load of 15 N without current applied and with 4 A current applied, respectively. The inset pictures were the optical images of the same balls. For the no current condition, it could be clearly seen in the optical image that most part of the ball surface was white, which indicates the exposure of the steel. And in the SEM image, it could be further confirmed

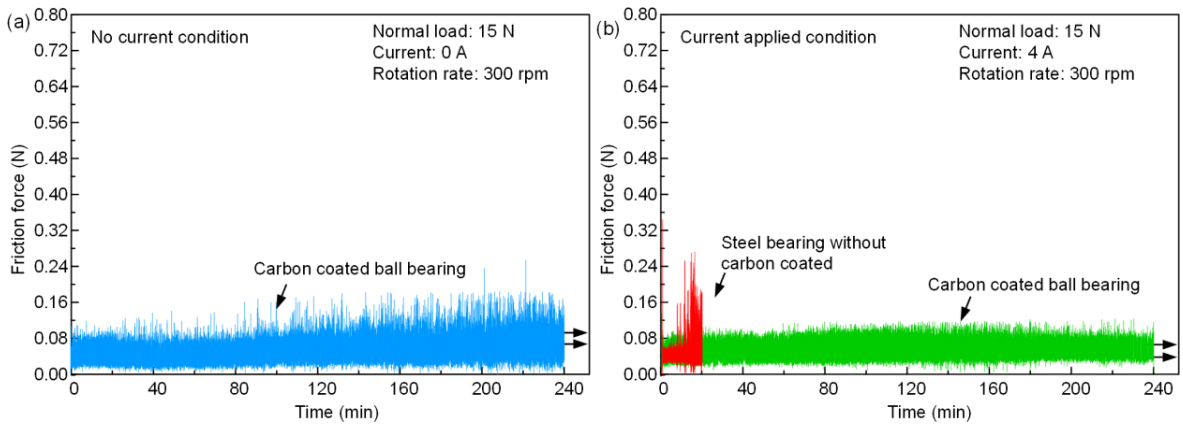


**Fig. 4** Friction force curves in wear stability tests. (a) Friction force curve of carbon coated ball bearing withour current applied. (b) Friction force curves of carbon coated ball bearing and pure steel ball bearing with current applied.

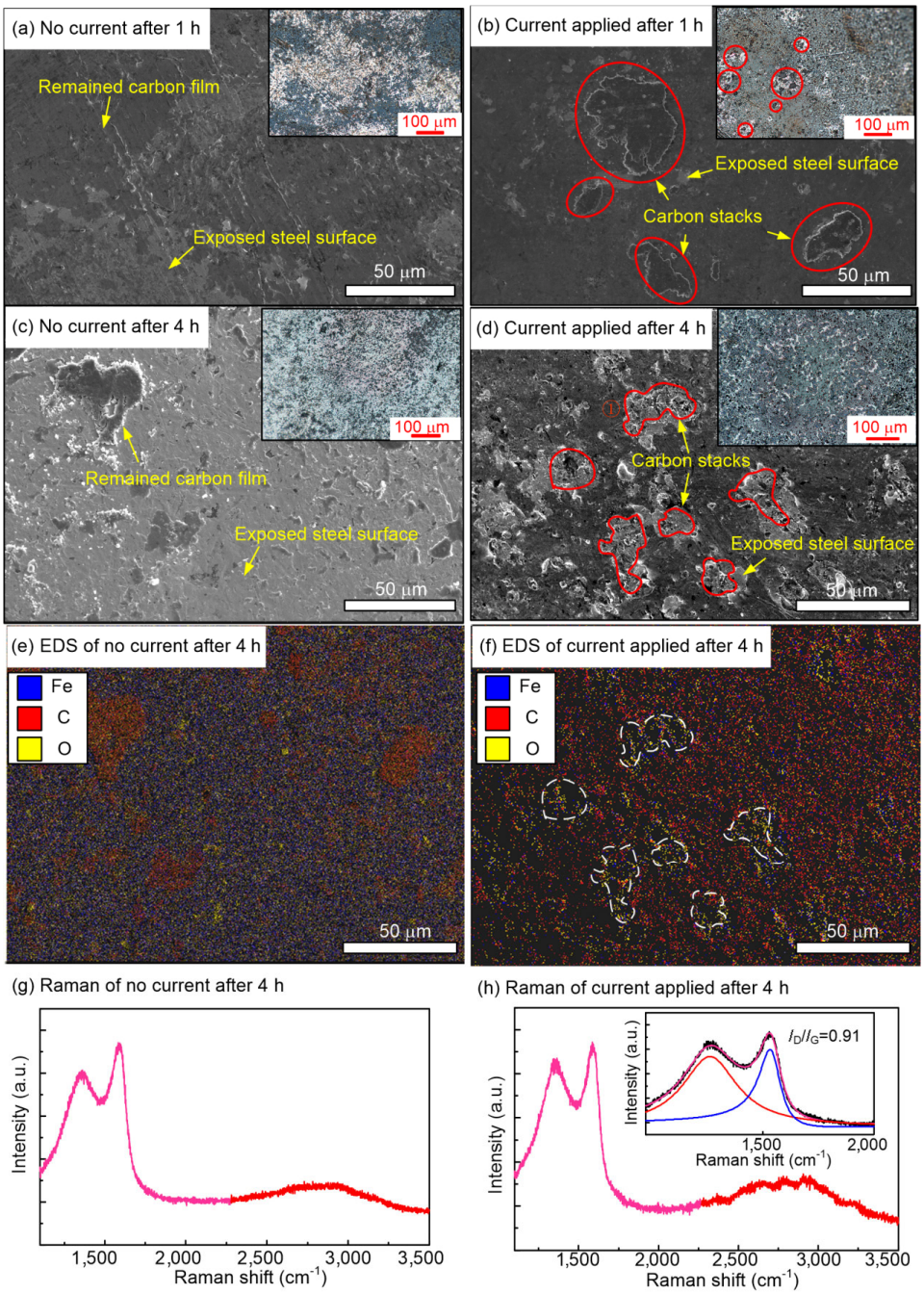


**Fig. 5** Characterizations of bearing ball surface after wear stability tests. SEM photos of the bearing ball surface after 1 h wear stability test (a) without current and (b) with current applied. (c) SEM photos of the bearing ball surface after 4 h wear stability test (c) without current applied and (d) with current applied. EDS analyses of the same area after 4 h wear stability test (e) without current applied and (f) with current applied. Raman spectra of the film on the ball surface after 4 h wear stability test (g) without current and (h) with current applied.

that only some small areas of the ball surface were covered with carbon film. However, when it came to the current-carrying condition, the worn surface became totally different. Most of the surface areas were still covered with carbon film and only some small white spots could be observed in the optical photo, indicating the exposure of steel. With further observation of the surface by using SEM in Fig. 5(d), it could be seen that some carbon stacks still remained in the worn area, as marked by the red circles. In order

to make the carbon stacks can be observed more clearly, an enlarged SEM photo of the area 1 marked in Fig. 5(d) was presented in Fig. S4 in the ESM.

Figures 5(e) and 5(f) exhibit the EDS analyses of the same area presented in Figs. 5(c) and 5(d), respectively. In the EDS images, the blue spots indicated the element of Fe, red spots indicated the element of C, and yellow spots indicated the element of O. For the no current condition presented in Fig. 5(e), most of the areas were blue and only a few areas were red, which means most of the carbon film has been worn out on the bearing ball surface. For the current-carrying condition presented in Fig. 5(f), most of the areas were still covered with red spots, which was in good accordance with the SEM image presented in Fig. 5(d). The areas marked with white dot lines were the same areas marked with red circles presented in Fig. 5(d). It was clear that the areas marked with white dot lines were filled with a majority of yellow spots, some red and blue spots, which was different from the worn out areas presented in Fig. 5(e). Considering the signal of Fe element in the white-circle-marked areas did not increase prominently comparing with that of the adjacent carbon film remained areas, it could be further confirmed that some carbon stacks still remained in the marked areas in Figs. 5(d) and 5(f). Independent element analyses of Figs. 5(c) and 5(d) were also presented in Fig. S5 in the ESM for a clearer observation.

Figures 5(g) and 5(h) presented the Raman spectra analyses of the remained carbon films after 4 h test without and with current applied, respectively. The spectrum presented in Fig. 5(g) was obtained from the remained carbon film on the ball, while spectrum presented in Fig. 5(h) was obtained from the carbon stacks as marked in red circles presented in Fig. 5(d). Comparing these with the Raman spectrum of the as-deposited carbon film presented in Fig. 2(d), the Raman spectra of the carbon film after wear stability test showed isolated D peak and G peak instead of a composite band of the as-deposited carbon film. For the no current condition, $I_D/I_G$ value increased from 0.72 to 0.78 comparing with that of the as-deposited film. For the current applied condition, $I_D/I_G$ increased from 0.72 to 0.91. The further increase of the $I_D/I_G$ indicated the formation of ordered nanocrystalline structrue under the current applied condition [24]. Besides the changes in D and G peak, the band ranges from 2,500 to 3,500 $cm^{-1}$ also changed. Some peaks could be identified around 2,700 $cm^{-1}$ in the Raman spectra of the carbon stacks. These peaks were considered to be the formation of few layers graphene [27]. Enlarged optical photos and Raman spectra of different positions on the ball surface after 4 h wear stability test were presented in Fig. S6 in the ESM, which were used to provide a more distinct observation of the carbon stacks in the optical photo and show the carbon compositions at different positions.

### *3.3.2 TEM and EDS analyses*

In order to further characterize the structure of the stacks, TEM photos were taken from a stack presented in Fig. 5(b). It was identified that the thickness of the as-deposited carbon was around 95 nm. And a much thicker carbon stack with a total thickness of 835 nm could be observed. The thickness of the carbon stack was more than 8 times thicker than that of the as-deposited carbon film, which could be observed in the low magnification photo in Fig. 6(a). The large thickness of the carbon stack should be understood as the aggregation of adjacent dropped carbon scarps, and may be also induced by the adsorption of O and H elements during current-carrying friction, which might form some C:H or C:H:O structures and lead to a low density structure like polymeric carbon [28]. Within the carbon stacks, both bright carbon area and dark steel area could be identified. It was noticed that also parts of the observed area were uniform structures, the rest parts still could be identified with many small spherical carbon scraps, which were marked by the blue circles. And the steel scarps were marked by red circles. Figure 6(b) presents the high magnification photo of the current applied condition. In the high magnification photo, two different crystal structures could be identified. The crystal structures marked by red circles had a relative small interplanar crystal spacing and more uniform lattice, which should be the crystal of Fe. While the crystal structure marked by blue circles had larger interplanar crystal spacing and were curved. These crystal structures should be the graphene nanocrystallites. The formation of those graphene nanocrystallites was owing to the applied current as well as the friction process [20].

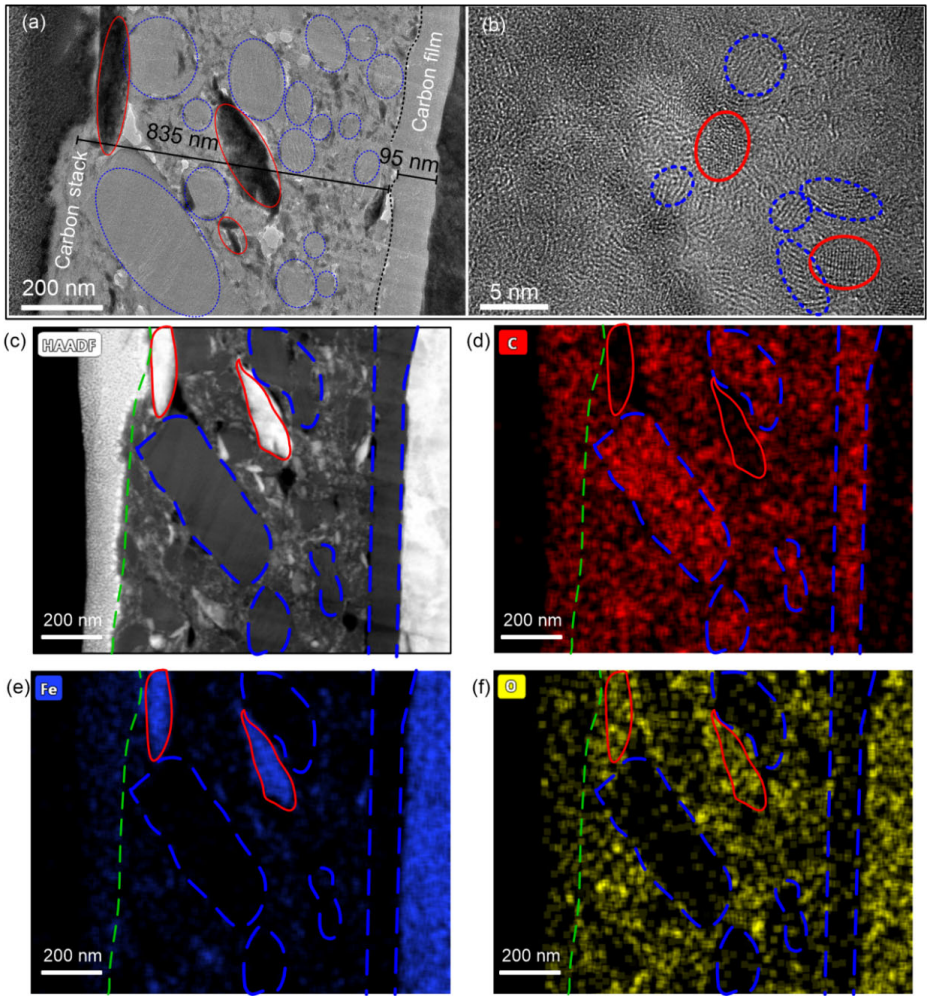


**Fig. 6** Characterizations of carbon stack. (a) Low and (b) high magnification images of the stack structure. (c) HADDF photo and EDS analyses of the same area of (d) C, (e) Fe, and (f) O elements.

Figures 6(c)–6(f) present the high-angle annular dark field (HAADF) photo as well as the EDS characterization of the same area as presented in Fig. 6(a). It is clear in the HAADF photo that black carbon scarps (marked with blue circles) and steel scarps (marked with red circles) are distributed in the stack. And the boundary between the stack and the deposited carbon film can be clearly observed. The EDS results confirmed the distribution of the C, Fe, and O elements as presented in both the TEM image and the HAADF photo. It was clear that carbon spread uniformly in the stack and the deposited carbon film except for the red circles marked areas. While the majority of Fe existed in the red circles marked areas and the steel ball, which was in accordance to the HADDF photo. The spread of O was very interesting. It could be concluded that except for the deposited carbon film and the carbon scraps marked with blue circles, O spread uniformly in all the rest area. The observation of the element distribution was in accordance with the results presented in Figs. 5(b) and 5(f). Thus, it could be concluded that the stacks on the surface were a mixture of large carbon scraps, oxide of carbon and small amount of steel scraps.

## 4 Discussions

The frictional results presented in this work showed that applying electric current can induce notable friction reduction and wear alleviation in the a-C carbon coated ball bearing system. The friction tests showed an instant reduction of the friction force when electrical current was applied with a maximum drop of 28%. And the wear stability tests showed that

comparing with no current situation, when current was applied to the carbon coated ball bearing system, a much more stable low friction force as well as less worn carbon film coated bearing balls could be obtained during the 4 h tests. Thus, the effects of the current on the friction reduction and wear alleviation in the carbon coated ball bearing system must be discussed and understood.

As for the friction reduction mechanisms for carbon film, two major theories have been postulated: (1) the formation of graphitization transfer film ("friction-induced graphitization" mechanism) [29, 30] and (2) the saturation of dangling bonds of carbon atoms at the friction interface (passivation mechanism) [31–33]. When it comes to the current applied friction situation, some researches on the steel/carbon counterparts have found that the current could facilitate the formation of transfer film with graphene sheets embedded structure [21], while other researches on graphite friction process found that the environment had a key influence on the friction coefficient, which indicates a passivation of the carbon dangling bonds [34]. And it was proved that when carbon film friction in the humid environment, surface passivation of –H and –OH could happen [35]. For the passivation mechanism, although friction process could help to form carbon dangling bonds, it still needs extra energy to promote the reaction between carbon atoms and gas atoms. The tribomicroplasma theory may provide a reasonable explanation for the tribo-chemistry process [36], which proved the generation of tribomicroplasma and emission of electrons and gas ions at the carbon film friction interface [37].

Thus, based on the experiment results in this work and the theories of former researches, a schematic diagram was proposed to understand the formation of carbon stacks and friction force reduction, as shown in Fig. 7. Figure 7(a) presents a local contact area at a certain moment. The contact area was presented at carbon stacks gathered area to help understand the friction process, and current would flow through the contact area. Figure 7(b) presents a more specific process of the friction reduction with carbon stacks formation. In order to explain the formation of carbon stacks and high amount of O, the tribomicroplasma theory was taken into account. The formation of the carbon stacks includes three major steps as the illustration presented. First, with the friction between the two contact surfaces, carbon scraps dropped from the surface and formed wear particles. Meanwhile, the friction process would also generate tribomicroplasma with electron and gas ions [36]. Then, the dropped wear particles would be charged with electrons and ions in the tribomicroplasma. Besides, the charge of wear particles could also be explained by the $H_2O$ dissociation at the current-carrying interface and combination of –OH and –H with wear particles [35]. When the dangling bonds on

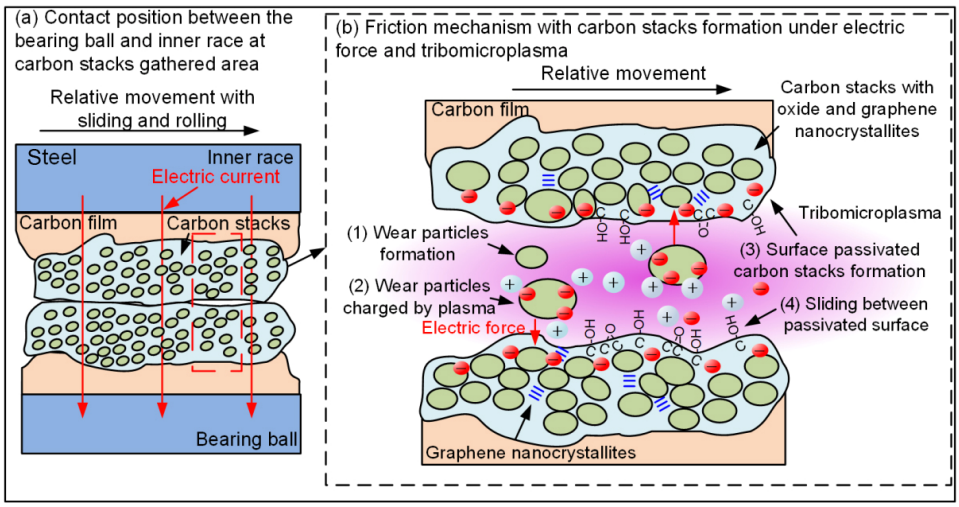


**Fig. 7** Current-carrying friction mechanisms. (a) Contact position between the bearing ball and inner race at carbon stacks gathered area. (b) Friction mechanism with carbon stacks formation under electric force and tribomicroplasma: (1) wear particles formation under friction force; (2) wear particles charged by tribomicroplasma; (3) wear particles attracted by electric force and surface passivated carbon stacks formation; and (4) sliding between passivated surfaces.

the newly exposed surface of wear particles attract and react with the gas ions or the dissociated water molecules, the electrical force can facilitate the particles stick to the place where they dropped. And as a result, the carbon stacks with oxide and graphene nanocrystallites formed on the contact interface, which was proved by the TEM results presented in Fig. 6. As for the high concentration of O in the stacks, two possible reasons can be considered. On one hand, it may come from the dissociation of $H_2O$ under current, which may form –OH and combine with carbon atoms [35]. On the other hand, some researches also indicated oxygen could be attracted to the interface under current-carrying friction condition and induce carbon atoms passivation with =O [38]. As for the formation of graphene nanocrystallites in the stacks, it should be induced by the combined effect of friction force and current [21, 39].

When we discuss the mechanisms of friction reduction in the current applied condition, it should be noticed that the contact points would change time by time in the ball bearing, which means the process inducing friction reduction must happen in a short time. One of the major reasons should be the passivation of the carbon dangling bonds with –OH or =O, which could provide a repelling force between the interface and reduce the adhesive force. And the graphene nanocrystallites formed at the interface as well as the spherical wear particles rolling in the interface could also lead to the friction reduction. As for the wear reduction of the carbon film on the bearing balls, it should be comprehended by a third-body process [40]. Under the current applied condition, the dropped wear particles would stay around where they dropped and form the carbon stacks due to the combined effect of tribomicroplasma and electric force, which could keep protecting the surface as a consequence. Besides, the reduced friction force by passivated surface can also alleviate the adhesive wear between the contact carbon films. As a result, current could further reduce the wear of the carbon materials on the ball surface as a result.

## 5 Conclusions

In summary, carbon coated ball bearings were fabricated with a rotatable substrate and the current-carrying friction behaviors and mechanisms in carbon coated ball bearings were studied. The current-carrying frictional tests showed the current could induce an instant and notable decrease of friction force with a maximum drop rate of 28% and significant wear alleviation. The SEM, TEM, and EDS results elucidated that the friction reduction mechanisms as follows: (1) wear particles formation; (2) wear particles charged by tribomicroplasma; (3) formation of surface passivated carbon stacks under electric force; (4) sliding between passivated surfaces. This work systematically studied the current carrying rolling friction in carbon coated ball bearings and laid some foundations for the development of novel solid lubricated ball bearings.

## Acknowledgements

The authors would like to thank the financial support of the National Natural Science Foundation of China (No. 51975383). The authors would like to thank Dr. Nan Jian, Dr. Meijie Yin, Xi Zhang in the Electron Microscope Center (EMC) of Shenzhen University for the help in TEM, SEM, and EDS characterizations with double spherical aberration corrected transmission electron microscope.

## Declaration of competing interest

The authors have no competing interests to declare that are relevant to the content of this article. The author Dongfeng DIAO is the Editorial Board Member of this journal.

**Electronic Supplementary Material:** Supplementary Material is available in the online version of this article at https://doi.org/10.1007/s40544-022-0704-8.

## References

[1] Tollefson J. Car industry: Charging up the future. *Nature* **456**(7221): 436–440 (2008)

[2] He R S, Ai B, Wang G P, Guan K, Zhong Z D, Molisch A F, Briso-Rodriguez C, Oestges C P. High-speed railway communications: From GSM-R to LTE-R. *IEEE Veh Technol Mag* **11**(3): 49–58 (2016)

[3] Slade P G. *Electrical Contacts: Principles and Applications*. CRC Press, 2017

[4] Zhao J, Peng Y T, Zhou Q G, Zou K. The current-carrying tribological properties of Cu/graphene composites. *J Tribol* **143**(10): 102101 (2021)

[5] Lang H J, Xu Y M, Zhu P Z , Peng Y T , Zou K, Yu K, Huang Y. Superior lubrication and electrical stability of graphene as highly effective solid lubricant at sliding electrical contact interface. *Carbon* **183**: 53–61 (2021)

[6] He F, Xie G X, Luo J B. Electrical bearing failures in electric vehicles. *Friction* **8**(1): 4–28 (2020)

[7] Krein P T. Electrostatic discharge issues in electric vehicles. *IEEE Trans Ind Appl* **32**(6): 1278–1284 (1996)

[8] Romanenko A, Muetze A, Ahola J. Effects of electrostatic discharges on bearing grease dielectric strength and composition. *IEEE Trans Ind Appl* **52**(6): 4835–4842 (2016)

[9] Suzumura J. Prevention of electrical pitting on rolling bearings by electrically conductive grease. *Quart Rep RTRI* **57**:42–47(2016)

[10] Fujishige M, Sekino M, Fujisawa K, Morimoto S, Takeuchi K, Arai S, Kawai A. Electric contact characteristic under low load of silver-carbon nanotube composite plating film corroded using $H_2S$ gas. *Appl Phys Express* **3**(6): 065801 (2010)

[11] Sundberg J, Mao F, Andersson A M, Wiklund U, Jansson U. Solution-based synthesis of AgI coatings for low-friction applications. *J Mater Sci* **48**:2236–2244 (2013)

[12] Akbulut H, Hatipoglu G, Algul H, Tokur M, Kartal M, Uysal M, Cetinkaya T. Co-deposition of Cu/WC/graphene hybrid nanocomposites produced by electrophoretic deposition. *Surf Coat Technol* **284**: 344–352 (2015)

[13] Robertson J. Diamond-like amorphous carbon. *Mater Sci Eng R Rep* **37**(4–6): 129–281 (2002)

[14] Hirono S, Umemura S, Tomita M, Kaneko R. Superhard conductive carbon nanocrystallite films. *Appl Phys Lett* **80**(3): 425–427 (2002)

[15] Sun K, Fan X, Yang L, Chen S C, Fan J, Diao D. Graphene nanocrystallites induced short run-in period with low electric power at current-carrying sliding interface. *Appl Surf Sci* **568**: 150902 (2021)

[16] Wang P, Yue W, Lu Z B, Zhang G G, Zhu L N. Friction and wear properties of $MoS_2$-based coatings sliding against Cu and Al under electric current. *Tribol Int* **127**: 379–388 (2018)

[17] Poljanec D, Kalinb M, Kumar L. Influence of contact parameters on the tribological behaviour of various graphite/graphite sliding electrical contacts. *Wear* **406–407**: 75–83 (2018)

[18] Csapo E, Zaidi H, Paulmier D. Friction behaviour of a graphite-graphite dynamic electric contact in the presence of argon. *Wear* **192**: 151–156 (1996)

[19] Bouchoucha A, Chekroud S, Paulmier D. Influence of the electrical sliding speed on friction and wear processes in an electrical contact copper–stainless steel. *Appl Surf Sci* **223**: 330–342 (2004)

[20] Sun K, Fan X, Zhang W Q, Xue P D, Diao D F. Contact-focusing electron flow induced nanosized graphene sheet formation in amorphous carbon films for fast low-friction. *Carbon* **149**: 45–54 (2019)

[21] Sun K, Diao D F. Current density effect on current-carrying friction of amorphous carbon film. *Carbon* **157**: 113–119 (2020)

[22] Fan X, Diao D F, Wang K, Wang C. Multi-functional ECR plasma sputtering system for preparing amorphous carbon and Al-O-Si films. *Surf Coat Technol* **206**(7): 1963–1970 (2011)

[23] Wang C, Diao D F, Fan X, Chen C. Graphene sheets embedded carbon film prepared by electron irradiation in electron cyclotron resonance plasma. *Appl Phys Lett* **100**(23): 231909 (2012)

[24] Ferrari A C, Robertson J. Interpretation of Raman spectra of disordered and amorphous carbon. *Phys Rev B* **61**(20): 14095–14107 (2000)

[25] Fan X, Diao D. Ion excitation and etching effects on top-surface properties of $sp^2$ nanocrystallited carbon films. *Appl Surf Sci* **462**: 669–677 (2018)

[26] Zaidi H, Chin K J, Frene J. Analysis of surface and subsurface of sliding electrical contact steel/steel in magnetic field. *Surf Coat Technol* **148**(2–3): 241–250 (2001)

[27] Wang C, Diao D F. Magnetic behavior of graphene sheets embedded carbon film originated from graphene nanocrystallite. *Appl Phys Lett* **102**(5): 052402 (2013)

[28] Chen X C, Zhang C H, Kato T, Yang X A, Wu S D, Wang R, Nosaka M, Luo J B. Evolution of tribo-induced interfacial nanostructures governing superlubricity in a-C: H and a-C: H: Si films. *Nat Commun* **8**: 1675 (2017)
[29] Liu Y, Meletis E I. An investigation of the relationship between graphitization and frictional behavior of DLC coatings. *Surf Coat Technol* **86–87**: 564–568 (1996)
[30] Voevodin A A, Phelps A W, Zabinski J S, Donley M S. Friction induced phase transformation of pulsed laser deposited diamond-like carbon. *Diam Relat Mater* **5**(11): 1264–1269 (1996)
[31] Konicek A R, Grierson D S, Sumant A V, Friedmann T A, Sullivan J P, Gilbert P U P A, Sawyer W G, Carpick R W. Influence of surface passivation on the friction and wear behavior of ultrananocrystalline diamond and tetrahedral amorphous carbon thin films. *Phys Rev B* **85**(15): 155448 (2012)
[32] Erdemir A. The role of hydrogen in tribological properties of diamond-like carbon films. *Surf Coat Technol* **146–147**: 292–297 (2001)
[33] Cui L C, Lu Z B, Wang L P. Probing the low-friction mechanism of diamond-like carbon by varying of sliding velocity and vacuum pressure. *Carbon* **66**: 259–266 (2014)
[34] Paulmier D, El Mansori M, Zaïdi H. Study of magnetized or electrical sliding contact of a steel XC48/graphite couple. *Wear* **203–204**: 148–154 (1997)
[35] Gharama A A, Lukitschb M J, Qi Y, Alpas A T. Role of oxygen and humidity on the tribo-chemical behaviour of non-hydrogenated diamond-like carbon coatings. *Wear* **271**: 2157–2163 (2011)
[36] Nakayama K, Nevshupa R A. Plasma generation in a gap around a sliding contact. *J Phys D*: *Appl Phys* **35**(12): L53–L56 (2002)
[37] Nakayama K. Triboemission of electrons, ions, and photons from diamondlike carbon films and generation of tribomicroplasma. *Surf Coat Technol* **188–189**: 599–604 (2004)
[38] Robert F, Csapo E, Zaidi H, Paulmier D. Influence of the current and environment on the superficial structure of a graphite electrical collector. *Int J Mach Tools Manuf* **35**(2): 259–262 (1995)
[39] Ma T B, Hu Y Z, Wang H. Molecular dynamics simulation of shear-induced graphitization of amorphous carbon films. *Carbon* **47**(8): 1953–1957 (2009)
[40] Singer I L. How third-body processes affect friction and wear. *MRS Bull* **23**(6): 37–40 (1998)

**Peidong XUE.** He received his Ph.D. degree in mechanical engineering from Xi'an Jiaotong University, China, 2021. He worked at the University of Kyoto from June 2019 to July 2020. He joined the Institute of Nanosurface Science and Engineering at Shenzhen University in August 2021, and now he is a post-doctor. His research interests include tribology, flexible sensor, and MEMS.

**Xue FAN.** She received her bachelor and Ph.D. degrees from Xi'an Jiaotong University in 2006 and 2012, respectively. She worked at the University of Tokyo from October 2010 to November 2011, and at Xi'an Jiaotong University from June 2012 to December 2014. She joined the Institute of Nanosurface Science and Engineering (INSE) at Shenzhen University in April 2015, and now she is an associate professor. Her research interests include the nanostructured carbon nanosurface, *in-situ* TEM friction and wear, and electron-carrying tribology.

**Dongfeng DIAO**. He obtained his Ph.D. degree in mechanical engineering from Tohoku University, Sendai, Japan, 1992. He currently is a distinguished professor and director for Institute of Nanosurface Science and Engineering (INSE) and Electron Microscope Center (EMC) at Shenzhen University, Shenzhen, China. He is a foreign member of the Engineering Academy of Japan (EAJ). His research interests include nanosurface science and technology, nanotriboelectronics, quantum tribology, and contact-electrification based sensor technology.